Applied Catalysis B: Environmental 142–143 (2013) 458–464

Contents lists available at SciVerse ScienceDirect

Applied Catalysis B: Environmental

journal homepage: www.elsevier.com/locate/apcatb

Enhanced visible-light photocatalytic properties of Fe^{3+}-grafted N-doped TiO_2 nanoporous spheres

Sher Bahadur Rawal, Hark Jin Kim, Wan In Lee*

Department of Chemistry, Inha University, Incheon 402-751, Republic of Korea

ARTICLE INFO

Article history:
Received 19 March 2013
Accepted 26 May 2013
Available online 31 May 2013

Keywords:
TiO_2
Nitrogen-doped TiO_2
Fe^{3+}-grafted
TiO_2 sphere
Photocatalyst
Visible-light
2-Propanol
Acetaldehyde
SiO_2 binder
CO_2 evolution

ABSTRACT

Monodispersed 250 nm-sized TiO_2 sphere (TiO_2 SP) with large internal surface area was successfully employed in fabricating the Fe^{3+}-grafted nitrogen-doped TiO_2 (Fe^{3+}/N-TiO_2), exhibiting ultra-high visible-light photocatalytic efficiency. In evolving CO_2 from the gaseous 2-propanol (IP) and acetaldehyde, the prepared Fe^{3+}/N-TiO_2 SP demonstrated twice of catalytic activity, comparing with the nanoparticle (NP)-based Fe^{3+}/N-TiO_2. Consequently, the optimized Fe^{3+}/N-TiO_2 SP exhibited 5.0–7.3 times higher efficiency than the bare N-TiO_2 NP. The instability of photocatalytic activity is a well-known drawback of the Fe^{3+}/N-TiO_2 system, caused by the inherent weakness of Fe^{3+} ions from the chemical attacks. Herein, however, it was found that SP system with large internal surface is remarkably advantageous for protecting the grafted Fe^{3+} ions. With mixing of 20 wt% silica binder, which is regarded to be a typical dosage for application, photocatalytic efficiency of the Fe^{3+}/N-TiO_2 SP was decreased by only 21–25%, whereas that of the NP-based sample was reduced by 73–80%.

1. Introduction

Photocatalytic decomposition of organic pollutants has attracted extensive attention for the last a few decades [1,2], and TiO_2 has been known as the most efficient photocatalytic material among various semiconductors due to its unique characteristics in band position, charge mobility, surface structure, chemical stability, etc. [3–8]. However, TiO_2 with band gap of 3.2 eV can only absorb the photons in the UV region ($\lambda \leq 380$ nm), which limits its commercial applications in sun light or indoor [9–13]. Thus, the design of photocatalysts functional under visible-light is essential in order to utilize the major portion of solar spectrum.

Recently, metal ion-grafted TiO_2 systems, which are sensitized by visible-light via charge-transfer reaction, have been fabricated [14–16], and they are now recognized as a promising strategy in designing visible-light photocatalysts. Irie and Hashimoto et al. reported several effective catalytic systems by grafting metal ions such as Cu^{2+} [17], Fe^{3+} [18], and Cr^{3+} [19] on the surface of TiO_2 or WO_3. They claimed that the photocatalytic reaction is initiated by the charge-transfer from the TiO_2 valence band (VB) to the metal ions by photons in visible range. For example, in Cu^{2+}/TiO_2 system, the electrons in VB of TiO_2 can be charge-transferred to the Cu^{2+} ions under visible-light irradiation, since the redox potential of Cu^{2+}/Cu^{+} and the VB edge of TiO_2 are +0.16 V (vs. NHE) and +2.7 V, respectively [20,21]. As a result, the holes generated in the VB of TiO_2 can be utilized for the photocatalytic oxidation reactions. It is deduced that the reduced Cu^{+} ions return back to the original Cu^{2+} ions by transporting the electrons to the oxygen species, as described in the following equations.

$$O_2 + e^- \rightarrow {}^{\bullet}O_2^-, \quad E_0 = -0.046\,V \tag{1}$$

$$O_2 + 2H^+ + 2e^- \rightarrow H_2O_2, \quad E_0 = +0.682\,V \tag{2}$$

Morikawa et al. [15,16] developed more efficient visible-light photocatalytic systems by grafting several metal ions onto the nitrogen-doped TiO_2 (N-TiO_2). They found that the co-loading of Fe, Cu or Pt ions significantly enhances the photocatalytic activity of N-TiO_2 in mineralizing the acetaldehyde into CO_2 and H_2O under visible-light.

In the present work, 250 nm-sized nanoporous N-TiO_2 sphere (SP) was employed in the formation of Fe^{3+}-grafted N-TiO_2 system to achieve ultra-high photocatalytic efficiency and to extend its chemical stability, as described in the Scheme 1a. The nanoporous SPs are expected to show several advantages in fabricating the metal ion-grafted catalytic systems, compared to the nanoparticles (NPs). The SP, prepared in this work, possesses relatively higher

* Corresponding author. Tel.: +82 32 8631026; fax: +82 32 8675604.
E-mail address: wanin@inha.ac.kr (W.I. Lee).

0926-3373/$ – see front matter © 2013 Elsevier B.V. All rights reserved.
http://dx.doi.org/10.1016/j.apcatb.2013.05.067

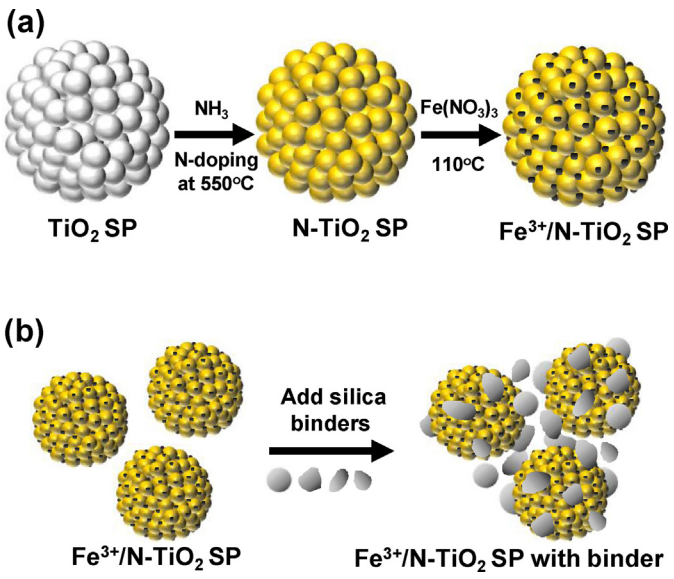

Scheme 1. Diagrams for the formation strategy of Fe^{3+}/N-TiO_2 SP (a) and the mixing of silica binder to the corresponding sample (b).

surface area than the typical NPs (Table 1). Moreover, it is a kind of assembled N-TiO_2 structure, which can induce efficient space-charge separation and are advantageous for multi-electrons/holes reactions. For example, Choi and co-workers [22] reported that the assembled TiO_2 structures exhibited considerably higher photocatalytic efficiency in producing H_2. Lakshminarasimhan et al. [23] also observed higher photocatalytic activity by using the agglomerated TiO_2 colloids. The enhanced photocatalytic activities could be rationalized by the charge separation facilitated by transfer of electrons among the TiO_2 grains within the agglomerates. Another noteworthy advantage of SP structure is in the possibility that the metal ions grafted on its internal surfaces are safely protected from the attack of chemical impurities or additives, due to the difficulty of their intrusion into the narrow pore channels. Thus the metal ion-grafted N-TiO_2 SP is expected to show extended chemical stability and long shelf-life under the presence of chemical impurities or additives.

In many applications, photocatalysts are fabricated as film-like structures on various substrates. For examples, they are applied as the coatings on window, wall of buildings, surface of ceramic tiles, plastics, textile, etc. For these applications, silica binders are generally mixed to the photocatalytic samples [24], because the introduction of silica binders contribute to form stable suspensions and also promote adhesion of the coated films to the substrate. Under this circumstance, the Fe^{3+}-grafted catalytic samples can be damaged by the added silica binders, since the photocatalytic sites of TiO_2 are screened by the binder and also the Fe^{3+} ions can be converted to other species by the chemical attack.

In the present work, the role of nanoporous spherical structures in enhancing the photocatalytic efficiency of Fe^{3+}/N-TiO_2 systems and the influence of added silica binders on their photocatalytic activities have been systematically investigated.

Table 1
Characterized results for TiO_2 NP, N-TiO_2 NP, TiO_2 SP, and N-TiO_2 SP.

Samples	Crystallite size (nm)	BET surface area (m^2g^{-1})	Internal pore size (nm)	Adsorbed IP (%)
TiO_2 NP	27.3	53.1	–	14.0
N-TiO_2 NP	33.2	51.5	–	16.8
TiO_2 SP	15.1	119.3	14.0	34.6
N-TiO_2 SP	23.4	104.1	14.0	34.8

2. Experimental

2.1. Preparation of nanoporous TiO_2 SPs

Nanoporous SP with a diameter of 250 nm was synthesized by a two-step process, consisting of controlled hydrolysis and subsequent hydrothermal reaction [25,26]. The sizes of the SP can be controlled by adjusting the TTIP/H_2O molar ratio (the *r*-factor). With the *r*-factor of 1/8, the diameter of the SP was controlled to 250 nm. Typically, 1 mmol methylamine and 48 mmol H_2O were added to a mixed solution of 50 mL ethanol (Aldrich) and 40 mL acetonitrile (Aldrich), and stirred for 5 min. Six millimoles titanium tetraisopropoxide (TTIP, Aldrich) stabilized in 10 mL ethanol was then added to this solution. The resultant solution, turned milky in a few seconds, was gently stirred for 1 h to obtain amorphous SP. The obtained SP were collected by centrifugation, and then transferred to a 0.3 L titanium bomb containing 70 mL H_2O and 70 mL ethanol. After a hydrothermal reaction at 230 °C for 5 h, the amorphous SPs were converted to highly porous and crystallized spherical structure. The prepared SPs were then collected by centrifugation, washed with ethanol several times, and dried at 100 °C.

2.2. Doping of nitrogen, grafting of Fe^{3+} ion, and mixing with silica binder

N-doped TiO_2 SP and NP were prepared by the following procedure [27,28]. Two grams of TiO_2 SP or NP were loaded in a 50 mL alumina boat, which was placed in a gas-tight tube furnace (Lindberg Inc., Model No. STF55356C). Pure NH_3 gas (Matheson Inc., 99%) was then flown with a rate of 0.7 L/min for 4 h, while the furnace temperature was maintained at 550 °C. From our previous experiment, it was found that the N-doped TiO_2 samples prepared at this condition exhibited the optimum visible-light photocatalytic activity in evolving CO_2 from 2-propanol (IP) [29].

Fe^{3+}/N-TiO_2 samples were prepared by impregnating the Fe^{3+} ions on the surface of N-TiO_2 by the following procedure [18]. One gram of N-TiO_2 SP or NP was dispersed in 50 mL ethanol, and the stoichiometric amounts of $Fe(NO_3)_3{\cdot}9H_2O$ (Aldrich) were dissolved to this suspension. The resultant suspensions were refluxed for 2 h, while vigorous stirring. The suspension was then filtered by centrifugation and washed twice with deionized water. The collected precipitate was dried at 120 °C for 24 h, and gently ground into fine powder in a mortar to form Fe^{3+}/N-TiO_2.

In order to evaluate the photocatalytic stability of the Fe^{3+}-grafted N-TiO_2 samples, a commercial silica binder was mixed, and the changes of photocatalytic activities were then analyzed. An analytical grade silica binder, containing 6 wt% silanol-functionalized SiO_2, was purchased from ChemWellTech Inc., and was used as received without further treatment. The amounts of silica binder mixed to the Fe^{3+}/N-TiO_2 powders were varied from 0 to 20 wt%. For example, to mix 20 wt% silicate binders, 3.3 g of the binder solution, containing 0.2 g SiO_2, was added to the 1.0 g Fe^{3+}/N-TiO_2 samples suspended in 10 mL ethanol. The mixture was stirred for 1 h, while heated at 90 °C, and then dried at 120 °C for 24 h.

2.3. Characterizations

X-ray diffraction (XRD) patterns were obtained for the N-TiO_2 and Fe^{3+}/N-TiO_2 powder samples by using a Rigaku Multiflex diffractometer with monochromatic light-intensity Cu K_α radiation. XRD scanning was performed under ambient conditions over 2θ region of 20–70° at a rate of 2°/min (40 kV, 20 mA). UV–visible diffuse reflectance spectra were acquired by a Perkin-Elmer Lambda 40 spectrophotometer. $BaSO_4$ was used as the reflectance standard. SEM images were observed by a field emission scanning electron microscope (FE-SEM, Hitachi S-4500). Field

emission transmission electron microscope (FE-TEM) images were obtained by a JEOL JEM2100F operated at 200 kV. One milligram of the synthesized particles was dispersed in 50 mL of ethanol, and a drop of the suspension was then spread on a holey amorphous carbon film deposited on the copper grid [30]. X-ray photoelectron spectroscopy (XPS) analyses of the samples were carried out in an ultrahigh vacuum (UHV) chamber with a base pressure of 5×10^{-9} Torr at room temperature. Photoemission spectra were recorded by a Sigma Probe Instrument (Thermo VG, U.K.) equipped with a standard monochromatic Al Kα excitation source ($h\nu$ = 1486.6 eV). The binding energy was calibrated by measuring a C 1s peak at 284.6 eV.

2.4. Evaluation of photocatalytic activity

The visible-light photocatalytic efficiencies of the photocatalytic samples were estimated by monitoring the decomposition of gaseous IP and acetaldehyde (CH_3CHO). An aqueous suspension containing 8.0 mg of each photocatalytic sample was spread on a 2.5 cm × 2.5 cm Pyrex glass in a film form and subsequently dried at room temperature. The gas reactor system, used for the photocatalytic activity measurement, has been described elsewhere [30]. The net volume of the gas-tight reactor was 200 mL, and the photocatalytic film was located at the center of the reactor. The entire area of the photocatalytic film (2.5 cm × 2.5 cm) was irradiated by a 300 W Xe lamp (Oriol) through a UV cut-off filter (≤422 nm, ZUL0422 ASAHI Co.) and a water filter to cut-off IR spectrum. After evacuation of the reactor, 1.6 μL of the IP (or acetaldehyde) diluted 1:9 in water was injected into the reactor. The initial concentration of gaseous IP (or acetaldehyde) in the reactor was maintained at 117 ppm in volume (ppmv). Thus the ultimate concentration of CO_2 evolved, for IP and acetaldehyde, will be 351 and 234 ppmv, respectively. The total pressure of the reactor was then increased to 750 Torr by the addition of oxygen gas. Under these conditions, the IP (or acetaldehyde) and H_2O remained in the vapor phase. After a certain duration of irradiation, 0.5 mL of the gas in the reactor was automatically picked up and sent to a gas chromatograph (Agilent Technologies, Model 6890N) using an auto sampling valve system. For CO_2 detection, a methanizer was installed between the GC column outlet and the FID detector.

3. Results and discussion

Fig. 1a shows SEM images of the as-prepared TiO_2 SP after a hydrothermal reaction at 230 °C for 5 h. The TiO_2 SP, synthesized with an *r*-factor (molar ratio of TTIP to H_2O) of 1/8, was uniform in size with a diameter of ~250 nm. TEM image in Fig. 1b indicates that the TiO_2 SP is highly porous structure [25,26]. The high resolution image in the inset of Fig. 1b indicates that the SP consists of the individual TiO_2 nanocrystals with a size of ~15 nm, and that the nano-sized internal pores seem to be formed among the individual TiO_2 nanocrystals.

Then the N-TiO_2 SP was prepared by flowing NH_3 gas to the as-prepared TiO_2 SP at 550 °C for 4 h [27,28]. SEM and TEM images in Fig. 1c and d, respectively, reveal that the size and shape of the prepared N-TiO_2 SP was not appreciably changed during the nitrogen doping at elevated temperature. The high resolution TEM image in the inset of 1d also suggests that the grain size of TiO_2 constituting the SP structure was not varied appreciably. For the control experiment, N-TiO_2 NP was also prepared by doping the nitrogen at the same condition to the Degussa P25 TiO_2 (Fig. 1e). The particle shape and size of the prepared N-TiO_2 NP, as shown in Fig. 1f, were not appreciably different from the bare P25 TiO_2.

The XRD patterns in Fig. 2 indicate that the prepared TiO_2 SP is in the pure anatase phase (JCPDS, No. 73-1764). By applying the Scherrer equation to the anatase (1 0 1) peak, the crystallite size was determined to be 15.1 nm, which is consistent with the grain size observed from the TEM images. By doping nitrogen, the peak positions of X-ray diffraction peaks were slightly shifted to higher angle from those of the bare TiO_2 SP (inset of Fig. 2), which is regarded to be the change in lattice parameter by doping of nitrogen into the oxygen sites [31,32]. The crystallite size, BET surface area, internal pore diameter, and others of the bare TiO_2 NP, N-TiO_2 NP, bare TiO_2 SP, and N-TiO_2 SP samples are listed in Table 1.

Chemical environment and doping level of the nitrogen in the N-TiO_2 samples were analyzed by monitoring the N 1s core levels with XPS. Three peaks with binding energies of 396, 400, and 402 eV were observed for the prepared N-TiO_2 SP and N-TiO_2 NP samples, as shown in Fig. 3a. It was proposed by Saha and Tompkins that the peak at 396 eV is assigned to be the atomic β-N, whereas the peaks at 400 and 402 eV originate from the molecularly chemisorbed γ-N_2 [33]. Thus the presence of the peak in 396 eV clearly indicates that significant amount of N is doped in the TiO_2 lattice. From N 1s XPS spectra, the total N concentrations in N-TiO_2 SP and N-TiO_2 NP were determined to be 1.46 and 1.10 at.%, respectively.

Fe^{3+} ions were then grafted onto the N-TiO_2 (Fe^{3+}/N-TiO_2) samples in order to enhance the visible-light photocatalytic activity. Fig. 4 shows UV–visible diffuse reflectance spectra for the bare TiO_2 SP, N-TiO_2 SP and 0.2 wt% Fe^{3+}-grafted N-TiO_2 SP. Significant extension of the absorption edge to the visible-light region was observed for the N-TiO_2 SP, displaying a pale yellow color [33,34]. By grafting 0.2 wt% Fe^{3+} ions onto the N-TiO_2 SP, as shown in the inset of Fig. 4, the reflectance was slightly decreased in the spectral range of 430–600 nm, which is regarded to be due to the charge-transfer from the VB of N-TiO_2 to Fe^{3+} ions [18,35].

XPS analysis was also carried out for the Fe^{3+}/N-TiO_2 SP and NP samples to determine the oxidation state of Fe ions present on the surface of N-TiO_2. High-resolution XPS spectra of the Fe 2p region for N-TiO_2 SP and NP samples, loaded with 0.2 and 0.1 wt% Fe^{3+} ions, respectively, are shown in Fig. 3b. The two XPS peaks, assigned as Fe $2p_{3/2}$ and $2p_{1/2}$ peaks, appear at the binding energies of 710.8 eV and 723.4 eV, respectively, clearly indicating the presence of the free Fe^{3+} ions [18,36] in both samples.

In order to analyze the distribution of Fe^{3+} ions in the internal pore of the N-TiO_2 SP structure, 0.2 wt% Fe^{3+}-grafted N-TiO_2 SP was sliced by ultramicrotomy technique. Its cross-sectional TEM image is shown in Fig. 5a, and the EDX elemental mapping image to the Fe was then obtained at the same area. It was observed that the Fe-mapping image in Fig. 5b is identical with the original TEM image (Fig. 5a), clearly indicating that the Fe ions are uniformly dispersed over the whole internal surfaces of SP. Considering that the most surfaces in the SP structure are inherent from the internal pores, it is deduced that the majority of Fe^{3+} ions in N-TiO_2 SP are grafted on the wall of internal pores.

The photocatalytic activities of Fe^{3+}-grafted N-TiO_2 NP and SP in evolving CO_2 from IP and acetaldehyde in gas phase were evaluated under a visible-light irradiation ($\lambda \geq 422$ nm). First, as shown in Fig. 6a, the N-TiO_2 SP demonstrates notably higher photocatalytic activity than the N-TiO_2 NP. The evolved CO_2 in 2 h was 15.5 ppm, whereas that of the N-TiO_2 NP was only 8.7 ppm. In principle, catalytic activity of the photocatalysts is influenced by several factors such as surface area, crystallinity, surface structure, defects, etc. As shown in Table 1, the surface area of N-TiO_2 SP is 2.02 times that of N-TiO_2 NP, and it is also found that the adsorption amount of IP molecules by N-TiO_2 SP is 2.07 times that of N-TiO_2 NP, suggesting that the adsorbed amount of IP is simply proportional to the surface area. Thus high surface area is regarded as one of the crucial factors in improving the visible-light photocatalytic activity of N-TiO_2 SP. Another advantage of SP structure would be inherent from its assembled structure, as Choi et al. reported that the aggregated TiO_2 structures can show better photocatalytic efficiency than the

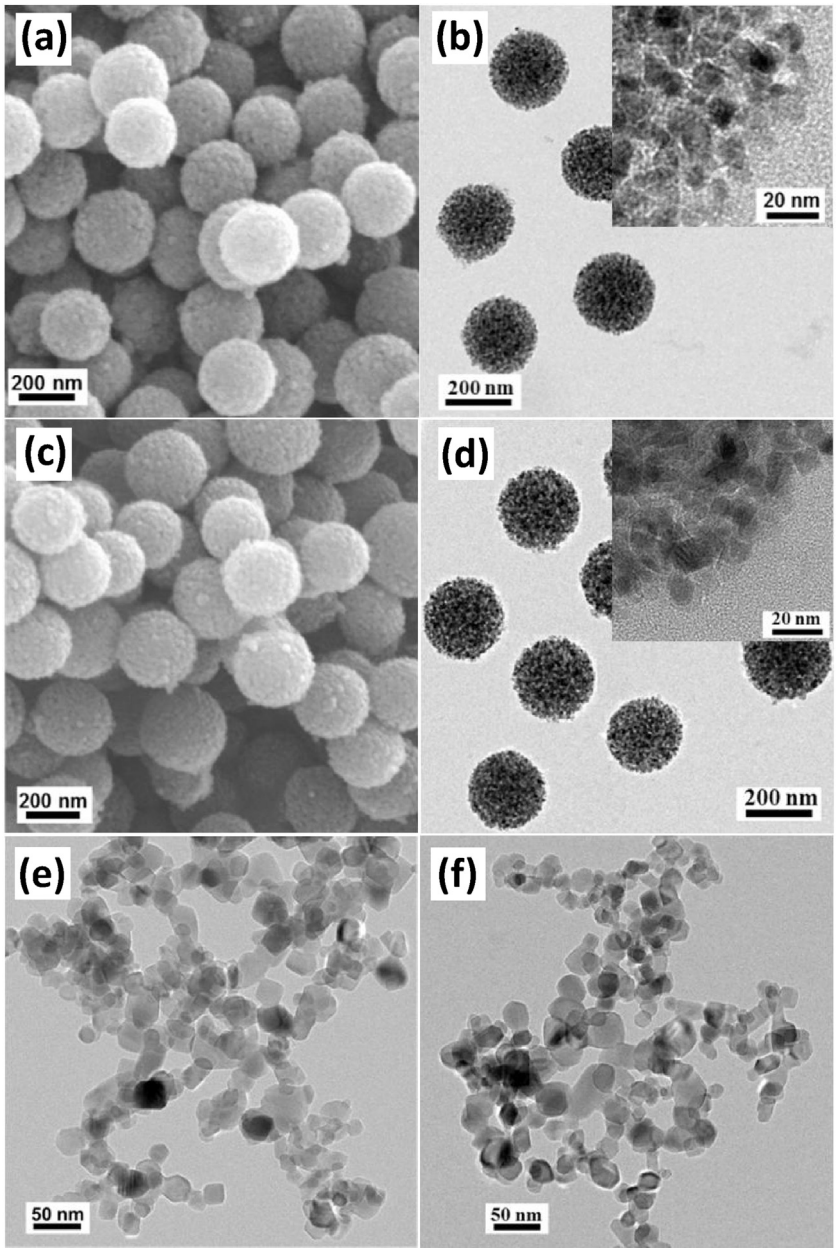

Fig. 1. SEM images of the bare TiO_2 SP (a) and N-TiO_2 SP (c), and TEM images of the bare TiO_2 SP (b), N-TiO_2 SP (d), bare TiO_2 NP (e) and N-TiO_2 NP (f). The magnified TEM images for the bare TiO_2 SP and N-TiO_2 SP are shown in the inset of (b) and (d), respectively.

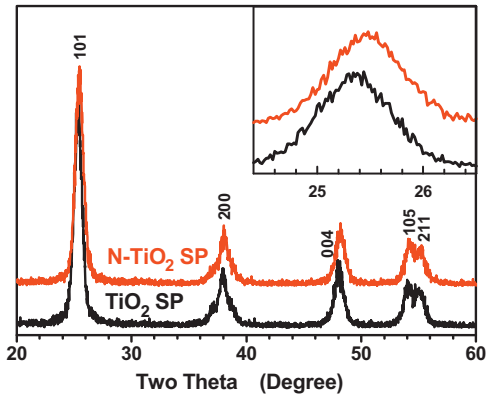

Fig. 2. XRD patterns of the bare TiO_2 SP and N-TiO_2 SP. The expanded anatase (1 0 1) peaks are included in the inset.

colloidal ones [21]. The large assembled structure of N-TiO_2 SP will be favorable for the space-charge separation of photo-induced electron–hole pairs, and the charge recombination could be suppressed as a result.

Second, the amounts of CO_2 evolved from IP in 2 h irradiation of visible-light with the Fe^{3+}-grafted N-TiO_2 NP and SP samples, as a function of Fe^{3+} concentration, are listed in Table 2. By grafting the Fe^{3+} ions, the amount of the evolved CO_2 was remarkably increased in both structures. In the NP-based system, the grafting of 0.1 wt% Fe^{3+} ions induced the optimized photocatalytic efficiency in evolving CO_2. The amount in 2 h was 22.3 ppmv, which was 2.5 times that of the bare N-TiO_2 NP. In contrast, in the SP-based system, the grafting of 0.2 wt% Fe^{3+} led to the highest photocatalytic efficiency, suggesting that the optimum level of Fe^{3+} is simply proportional to the surface area of N-TiO_2, considering that the surface area of N-TiO_2 SP is 2.02 times that of N-TiO_2 NP. The CO_2 evolved in 2 h with Fe^{3+}/N-TiO_2 SP was 43.8 ppmv, which is 2.8 times that of the

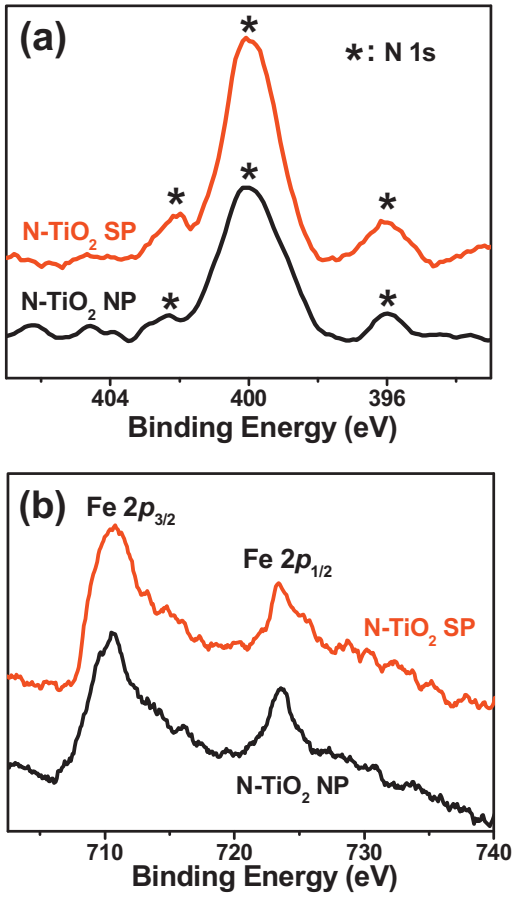

Fig. 3. N 1s XPS spectra for N-TiO_2 SP and N-TiO_2 NP (a), and Fe 2p XPS spectra for the 0.2 wt% Fe^{3+}/N-TiO_2 SP and 0.1 wt% Fe^{3+}/N-TiO_2 NP (b).

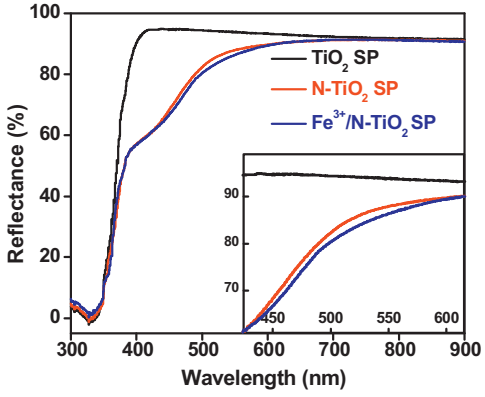

Fig. 4. Diffuse reflectance spectra of the bare TiO_2 SP, N-TiO_2 SP, and Fe^{3+}/N-TiO_2 SP. The enlarged spectra in the range of 425–625 nm are shown in the inset.

Table 2
Photocatalytic efficiencies of Fe^{3+}-grafted N-TiO_2 NP and SP. The amounts of evolved CO_2 in 2 h visible-light irradiation were monitored.

Catalytic systems	Fe^{3+} level (wt%)	Evolved CO_2 (ppm)	
		IP	Acetaldehyde
N-TiO_2 NP	0.0	8.7	9.9
	0.05	18.9	29.1
	0.10	22.3	35.3
	0.20	19.8	31.9
N-TiO_2 SP	0.0	15.5	19.9
	0.10	33.7	65.1
	0.20	43.8	72.2
	0.30	38.4	66.8

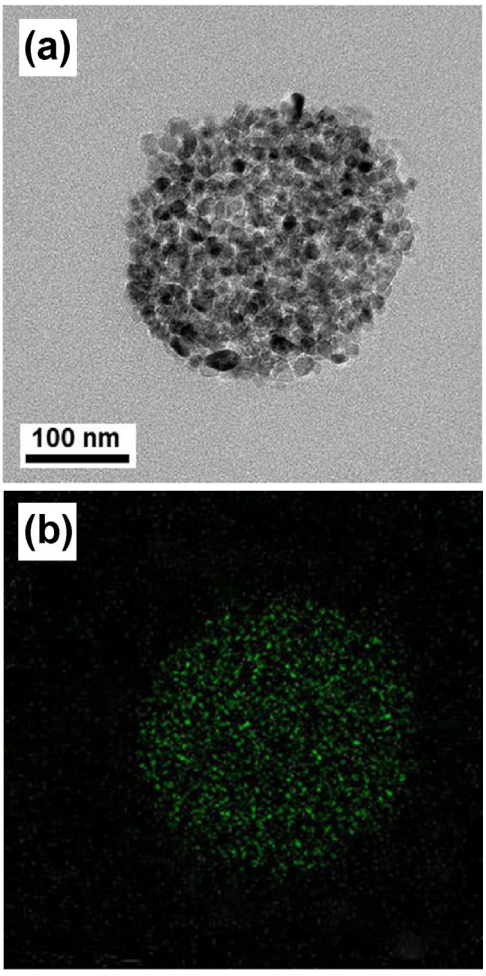

Fig. 5. TEM image for the cross-section of an Fe^{3+}/N-TiO_2 SP sliced by ultramicrotomy technique (a), and Fe elemental mapping image for the corresponding sample (b).

bare N-TiO_2 SP and ~2.0 times that of the Fe^{3+}/N-TiO_2 NP, as shown in Fig. 6a and Table 2.

The photocatalytic efficiencies of Fe^{3+}/N-TiO_2 NP and SP were also evaluated by monitoring the decomposition of gaseous acetaldehyde. Table 2 shows the evolved amounts of CO_2 with Fe^{3+}/N-TiO_2 NP and SP in different compositions. In decomposing acetaldehyde, it was also found that the optimum concentrations of Fe^{3+} ion for N-TiO_2 NP and SP were 0.1 and 0.2 wt%, respectively. As shown in Fig. 6b and Table 2, the evolved CO_2 in 2 h irradiation with the optimized Fe^{3+}/N-TiO_2 NP and Fe^{3+}/N-TiO_2 SP composites were 35.3 and 72.2 ppmv, respectively, whereas the bare N-TiO_2 NP and SP showed only 9.9 and 19.9 ppmv, respectively.

The mechanism for the catalytic activity enhancement with grafting of Fe^{3+} ions was initially proposed by Irie and Hashimoto et al. [17]. Nosaka and co-workers [35] also confirmed the proposed mechanism by electron spin resonance (ESR) spectroscopy. With visible-light irradiation, the electrons in VB of the bare TiO_2 or N-TiO_2 can be charge-transferred to the Fe^{3+}, since the energy gap between the redox potential of Fe^{3+}/Fe^{2+} (+0.7 V, vs. NHE) and the VB of TiO_2 (+2.7 V, vs. NHE) is 2.0 eV. By this charge transfer reaction, Fe^{3+} ions are reduced to Fe^{2+}, while the holes generated in the VB of N-TiO_2 participate in the photocatalytic oxidation reactions. Presumably the electrons in Fe^{2+} ions can be consumed in the reaction to form H_2O_2, as described in the Eq. (2), and the Fe^{3+} ions are regenerated as a result.

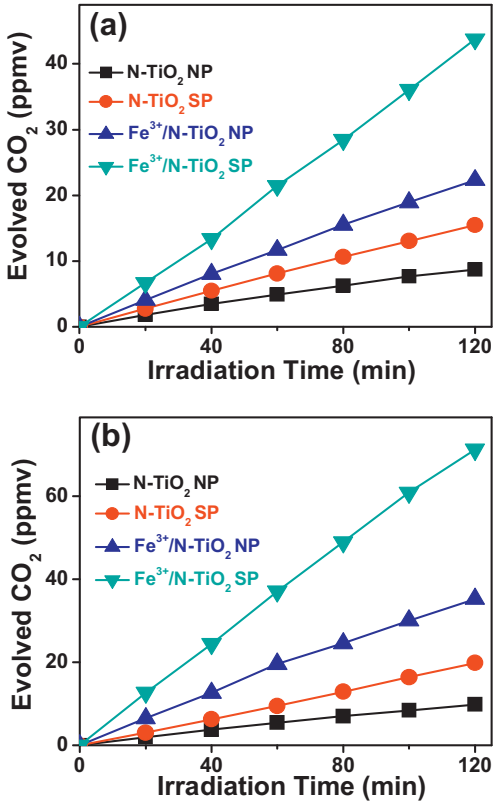

Fig. 6. The amounts of CO_2 evolved as a function of visible-light ($\lambda \geq 422$ nm) irradiation time with several photocatalytic samples in decomposing IP (a) and acetaldehyde (b).

Grafting of Fe^{3+} ions on the surface of TiO_2 greatly enhances the visible-light photocatalytic activity, as we have demonstrated, but the Fe^{3+}/N-TiO_2 system reveals a critical drawback in the chemical stability. That is, the photocatalytic activity can be diminished by the added impurities, since the Fe^{3+} ions are vulnerable to the attack from other chemicals. Moreover, thermal treatment or long-term storage can modify the Fe^{3+} ions to other chemical species, resultantly deteriorating the photocatalytic efficiency.

In applications, photocatalysts are commonly fabricated as film-like structures on various substrates, and the silica binders are usually mixed to the photocatalytic samples to improve the adhesion onto the substrate. During these essential procedures for applications, the Fe^{3+}-grafted catalytic systems might be damaged by the added silica binders. That is, photocatalytic sites of TiO_2 can be screened by the added binder, and the Fe^{3+} ions may also be converted to other chemical species. In this point of view, SP structure will be an advantageous template for grafting the metal ions on its surface, since the SP is highly porous structure with large internal surfaces. As shown in Scheme 1b, the silica binders, mostly consisting of SiO_2 NP, cannot penetrate into the internal pore of SP structures, because the average diameter of pore channel (~15 nm) is smaller than that of the SiO_2 NP in the silica binder. Thus only the external surface of N-TiO_2 surface is damaged by silica binder, and the internal surface, occupying the majority of SP surface, will not be contaminated by the added silica binder.

In order to examine the influence of the silica binder added to the Fe^{3+}-grafted photocatalytic samples, various amounts of silica binder were mixed with the Fe^{3+}/N-TiO_2 NP and Fe^{3+}/N-TiO_2 SP. The added silica binder consists of 20–30 nm-sized SiO_2 NPs and amorphous silica sol-gel, as shown in TEM image of Fig. 7. The visible-light photocatalytic efficiencies were then monitored by varying the added amounts of silica binder. For the

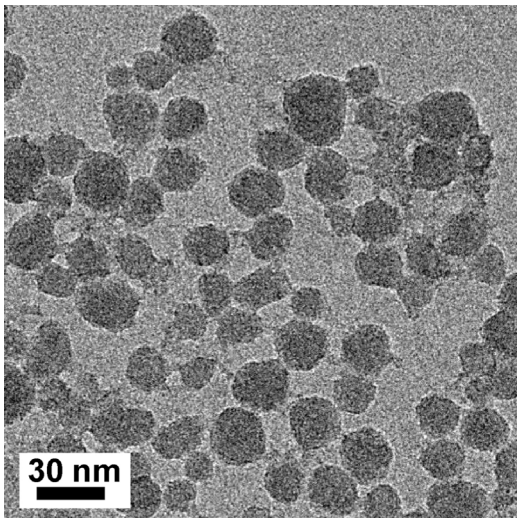

Fig. 7. TEM image of the silica binder mixed to the Fe^{3+}/N-TiO_2 samples.

Fe^{3+}/N-TiO_2 NP samples, the evolved CO_2 in 2 h from the decomposition of IP was sharply decreased, with increasing the added silica binder, as shown in Fig. 8a, The mixing of 20 wt% silica binder, which is regarded to be a typical dosage for application, dramatically decreased the CO_2 evolution from 22.3 to 5.4 ppm (~80% decrease). Contrarily, the photocatalytic efficiency of Fe^{3+}/N-TiO_2

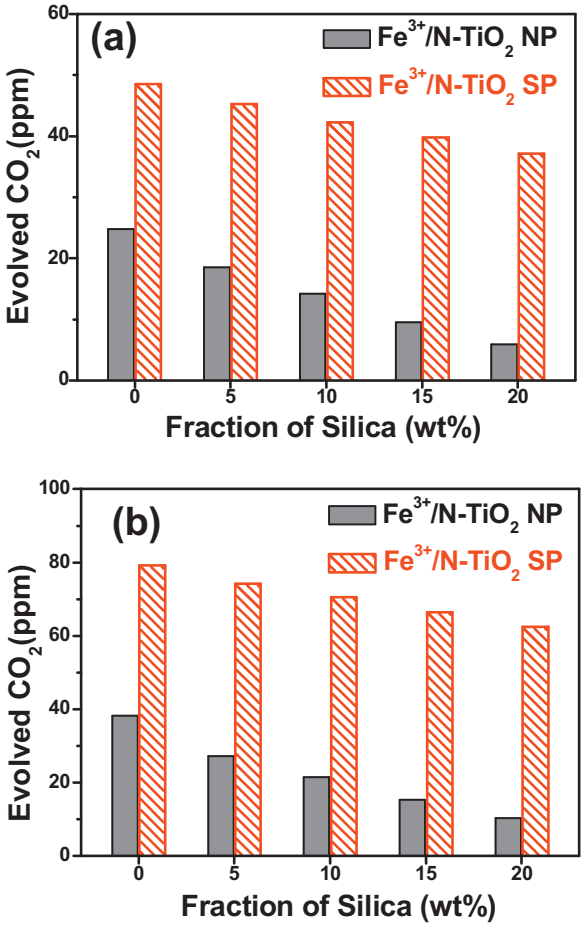

Fig. 8. The amounts of CO_2 evolved in 2 h for the Fe^{3+}/N-TiO_2 SP and NP, according to the amounts of the mixed silica binder, in decomposing IP (a) and acetaldehyde (b).

SP samples was not much influenced: The mixing of 20 wt% silica binder decreased the CO_2 evolution from 43.8 to 33.4 ppm (~25% decrease). Similar result was also observed in the decomposition of acetaldehyde, as shown in Fig. 8b. For the Fe^{3+}/N-TiO_2 SP, the amount of CO_2 evolved in 2 h was decreased by only 21% by mixing of 20 wt% silica binder, whereas that of Fe^{3+}/N-TiO_2 NP was decreased by ~73%. As a result, with mixing 20 wt% silica binder, the Fe^{3+}/N-TiO_2 SP system demonstrates ~6 times higher photocatalytic activity than the typical Fe^{3+}/N-TiO_2 NP system. The observed results demonstrate that nanoporous spherical TiO_2 structures have tremendous advantages in fabricating the Fe^{3+}/N-TiO_2 visible-light photocatalysts, both in catalytic activity and chemical stability. Therefore, nanoporous spherical structure will be a key template for obtaining highly efficient metal ion-grafted N-TiO_2 systems and also for their commercialization in the future.

4. Conclusions

Highly monodispersed 250 nm-sized N-TiO_2 SP with a surface area of 104.1 m^2g^{-1} exhibited great advantages in preparing Fe^{3+}-grafted nitrogen-doped TiO_2. In evolving CO_2 from the gaseous IP or acetaldehyde under visible-light irradiation ($\lambda \geq 422$ nm), the Fe^{3+}/N-TiO_2 SP demonstrated twice of catalytic activity than the NP-based Fe^{3+}/N-TiO_2. High surface area is regarded as one of the major factors in determining the enhanced visible-light photocatalytic activity of the Fe^{3+}/N-TiO_2 SP. Furthermore, the SP systems with large internal surfaces demonstrated considerably extended chemical stability: With mixing of 20 wt% silica binder, the photocatalytic efficiency of was decreased by only 21–25%, whereas that of Fe^{3+}/N-TiO_2 NP was reduced by 73–80%. It is deduced that the extended chemical stability of Fe^{3+}/N-TiO_2 SP is caused by its characteristic structure with narrow internal pore channel, preventing the penetration of silica binder into its internal pores. As a result, with mixing of silica binder, Fe^{3+}/N-TiO_2 SP system demonstrates ~6 times photocatalytic activity, compared to Fe^{3+}/N-TiO_2 NP.

Acknowledgments

This work has been supported by the National Research Foundation of Korea (Project No. 2011-0028981), and Korea Center for Artificial Photosynthesis (KCAP) funded by the Ministry of Education, Science, and Technology (NRF-2012M1A2A2671781).

References

[1] A. Heller, Acc. Chem. Res. 28 (1995) 141.
[2] A. Fujishima, K. Hashimoto, T. Watanabe, TiO_2 Photocatalysis, Fundamentals and Applications, BKC Inc., Tokyo, 1999.
[3] T. Inoue, A. Fujishima, S. Konishi, K. Honda, Nature 277 (1979) 637.
[4] M.R. Hoffmann, S.T. Martin, W. Choi, D.W. Bahnemann, Chem. Rev. 95 (1995) 69.
[5] E.S. Jang, J.H. Won, S.J. Hwang, J.H. Choy, Adv. Mater. 18 (2006) 3309.
[6] Z. Ding, G.Q. Lu, P.F. Greenfield, J. Phys. Chem. B 104 (2000) 4815.
[7] Y. Ou, J. Lin, S. Fang, D. Liao, Catal. Commun. 8 (2007) 936.
[8] Y. Huang, Z. Ai, L. Zheng, X. Zhang, Z. Fan, Zou, J. Phys. Chem. B 110 (2006) 19323.
[9] C. Burda, Y. Lou, X. Chen, A.C.S. Samia, J. Stout, J.L. Gole, Nano Lett. 3 (2003) 1049.
[10] V. Stengl, V. Houskova, S. Bakardjieva, N. Murafa, ACS Appl. Mater. Interfaces 2 (2010) 575.
[11] S. Klosek, D. Raftery, J. Phys. Chem. B 105 (2001) 2815.
[12] S. Sakthivel, H. Kisch, Chem. Phys. Chem. 4 (2003) 487.
[13] H. Tada, M. Fujishima, H. Kobayashi, Chem. Soc. Rev. 40 (2011) 4232.
[14] A.D. Paola, E.G. Lopez, G. Marc, C. Martin, L. Palmisano, V. Rives, A.M. Venezia, Appl. Catal. B: Environ. 48 (2004) 223.
[15] T. Morikawa, Y. Irokawa, T. Ohwaki, Appl. Catal. A: General 314 (2006) 123.
[16] T. Morikawa, T. Ohwaki, K.I. Suzuki, S. Moribe, S.T. Kubota, Appl. Catal. B: Environ. 83 (2008) 56.
[17] H. Irie, S. Miura, K. Kamiya, K. Hashimoto, Chem. Phys. Lett. 457 (2008) 202.
[18] H. Yu, H. Irie, Y. Shimodaira, Y. Hosogi, Y. Kuroda, M. Miyauchi, K. Hashimoto, J. Phys. Chem. C 114 (2010) 16481.
[19] H. Irie, T. Shibanuma, K. Kamiya, S. Miura, T. Yokoyama, K. Hashimoto, Appl. Catal. B: Environ. 96 (2010) 142.
[20] H. Irie, K. Kamiya, T. Shibanuma, S. Miura, D.A. Tryk, T. Yokoyama, K. Hashimoto, J. Phys. Chem. C 113 (2009) 10761.
[21] C.R. Weast (Ed.), Handbook of Chemistry and Physics, 77th ed., CRC Press, Boca Raton, FL, 1996.
[22] N. Lakshminarasimhan, A.D. Bokare, W. Choi, J. Phys. Chem. C 116 (2012) 17531.
[23] N. Lakshminarasimhan, W. Kim, W. Choi, J. Phys. Chem. C 112 (2008) 20451.
[24] J. Oguma, Y. Kakuma, M. Nishikawa, Y. Nosaka, Catal. Lett. 142 (2012) 1474.
[25] Y.J. Kim, M.H. Lee, H.J. Kim, G.I. Lim, Y.S. Choi, N.G. Park, K.K. Kim, W.I. Lee, Adv. Mater. 21 (2009) 3668.
[26] I.G. Yu, Y.J. Kim, H.J. Kim, C.M. Lee, W.I. Lee, J. Mater. Chem. 21 (2011) 532.
[27] T. Morikawa, T. Ohwaki, K. Suzuki, S. Moribe, S.T. Kubota, Appl. Catal. B: Environ. 83 (2008) 56.
[28] H. Irie, Y. Watanabe, K. Hashimoto, J. Phys. Chem. B 107 (2003) 5483.
[29] S.B. Rawal, A.K. Chakraborty, Y.J. Kim, H.J. Kim, W.I. Lee, RSC Adv. 2 (2012) 622.
[30] Y.T. Kwon, K.Y. Song, W.I. Lee, G.J. Choi, Y.R. Do, J. Catal. 191 (2000) 192.
[31] D. Chen, Z. Jiang, J. Geng, Q. Wang, D. Yang, Ind. Eng. Chem. Res. 46 (2007) 2741.
[32] T.C. Jagadale, S.P. Takale, R.S. Sonawane, H.M. Joshi, S.I. Patil, B.B. Kale, S.B. Ogale, J. Phys. Chem. C 112 (2008) 14595.
[33] N.C. Saha, H.G. Tompkins, J. Appl. Phys. 72 (1992) 3072.
[34] R. Asahi, T. Morikawa, T. Ohwaki, K. Aoki, Y. Taga, Science 293 (2001) 269.
[35] M. Nishikawa, Y. Mitani, Y. Nosaka, J. Phys. Chem. C 116 (2012) 14900.
[36] G.K. Mor, H.E. Prakasam, O.K. Varghese, K. Shankar, C.A. Grimes, Nano Lett. 7 (2007) 2356.